BNL FAST SHAVING EXTRACTION SYSTEM*

L. Blumberg, G. Bagley, G. Bennett, J. Claus, J. Curtiss, R. Frankel,
H. Hsieh, J. Keane, G. Levine, L. Repeta, J. Schuchman, A. Soukas
Brookhaven National Laboratory
Upton, New York

Summary

Design and performance of a recently commissioned fast extraction system to serve the requirements of the bubble chamber programs at the AGS are discussed. Several of the major components are described along with the diagnostic instrumentation and system performance. Extraction of various fractions of the internal beam, including total extraction in an essentially single-turn mode, has been accomplished with the AGS beam either bunched or debunched. The expected extraction efficiency, ~ 95%, has been observed and transport losses in the 258 m, 10-cm aperture external beam are ≤ 1 %.

I. Shaving Extraction Method

In a previous paper,[1] we presented the orbit calculations, configuration and component parameters of the extraction system. A similar system has been developed at CERN[2] for extraction from the PS. Briefly, the method consists of producing a rapid, local orbit deformation at the azimuth of a thin septum magnet in straight section E10. The fraction of beam displaced across the septum is deflected into the aperture of a septum ejector magnet at straight section H10, approximately 2½ betatron wavelengths (λ_β) from E10. The rapid orbit deformation is produced by two full aperture, single-turn, ferrite core kicker magnets located in straight sections C15 and E15 with a separation of approximately 1½ λ_β. In the fractional extraction mode, the kickers are powered by a half sinusoid current waveform of 2.5 μs duration. For full extraction, the waveform duration is ~ 6 μs with amplitude of ~ 8000 A. At 5000 A in the kickers, and at typical extraction momentum 28.7 GeV/c, the measured deflection at E10 is 1.4 cm, which is adequate for complete displacement of a 1.3 cm wide[3] AGS bunch across the 0.3 mm E10 septum. A 1.0 mrad deflection at E10, provided by a current pulse of 3000 A peak and 200 μs duration in the single-turn magnet deflects the shaved fraction across the 2.25 mm H10 ejector septum with a measured separation between circulating and shaved beam of 7.6 mm, in good agreement with calculations. The H10 ejector, also a single turn magnet, provides a 1.5 ms current pulse of 21,000 A peak, and deflects the beam by 22 mrad into the external channel for the 7-ft bubble chamber neutrino beam. The E10 and H10 septa are fixed at mean radial positions relative to the AGS central orbit of 4.6 and 5.6 cm respectively, during the entire accelerating cycle; slower orbit deformations of 9 ms duration in a 1/2 λ_β configuration centered at the septa are energized prior to extraction and provide measured displacements of 3.95 and 3.7 cm at E10 and H10 respectively, for a 1000 A peak current through backleg windings on selected AGS magnets. We have determined that the septa are not machine apertures at injection energy, even for intensities up to 9×10^{12} protons/pulse.

Another operating mode, presently being commissioned, involves a polarity reversal of the H10 magnet and deflection of the shaved beam by -3 mrad, back into the AGS aperture, for extraction 3/4 λ_β downstream at I10 for the 80-in. bubble chamber. The I10 ejector magnet, originally used for single-bunch extraction,[4] has been reduced in septum thickness to 2.0 cm and a backleg winding 1/2 λ_β orbit deformation has been deployed in the I superperiod for the present application. In this mode, we will extract only ~ 2% of the 6×10^{12} p/p circulating beam; the system is capable of four extractions per second at 200 ms intervals. We have achieved the required spill duration of ≤ 1.5 μs imposed by the present pulse duration of the rf beam separator for the 80-in. chamber. Also, we have extracted the beam both during the acceleration and flat top part of the AGS cycle.

II. Extraction Components

Kicker Power Supply

For the fractional shaving mode, a deuterium thyratron switches a 0.2 μF capacitor charged to 30 kV, generating a 5 kA peak pulse with 2.5 μs base. In the full extraction mode, four thyratrons are triggered, each switching a 0.2 μF capacitor at 30 kV onto the common load. Two thyratrons are triggered initially; 0.6 μs later, the other two are triggered. The resulting pulse has an 8 kA amplitude and 0.5 μs rise time with 6 μs base. This triggering method produces an optimum waveshape for the given constants of cable and magnet.

Ejector Power Supply

The H10 magnet supply consists of an energy discharge system in which magnet inductance and power supply capacitance oscillate with a period of 3 ms. The stored energy is 5500 J and the peak current is 21.5 kA at 800 V. The power supply is completely solid state, featuring water cooled SCR's (thyristors) and silicon rectifiers. The charging supply is a three phase, constant current type utilizing resonant monocyclic networks. This system eliminates the need for a lossy series charging resistor.

Ejector Magnet

The ejector magnet, located at the H10 straight section, has been designed to serve two purposes. The magnet assembly consists of two segments; the length ratio is one-third for the upstream segment and two-thirds for the downstream segment. With a current of 21.5 kA flowing in the same direction in both segments, the beam is deflected 22 milliradians out of the AGS, aiming toward the 7 ft. chamber. With a current of 8 kA flowing in the opposite direction in the downstream segment, the beam is displaced across a thick septum (20 mm) at the I10 straight section. A further kick by the I10 ejector magnet causes the beam to exit from the AGS aiming toward the 80-in. bubble chamber.

*Work performed under the auspices of the U.S. Atomic Energy Commission.

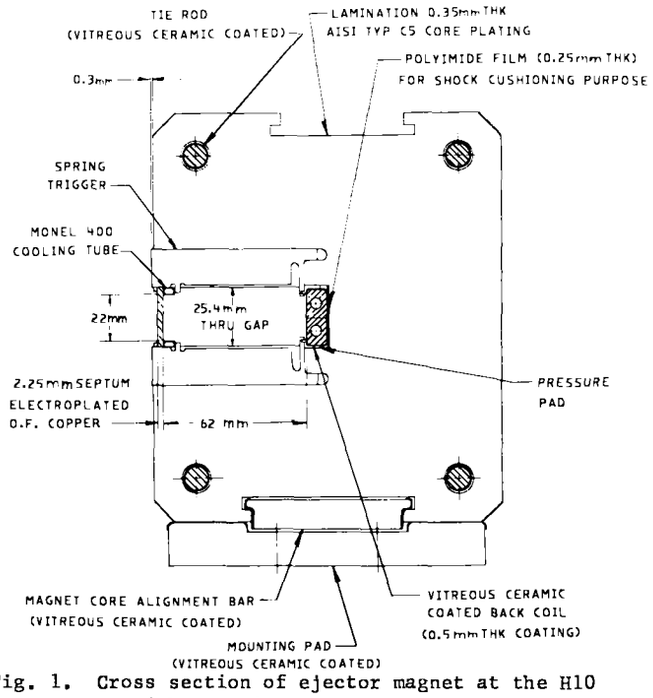

Fig. 1. Cross section of ejector magnet at the H10 straight section.

The cross section of the magnet is shown in Fig. 1. The septum is of copper 2.25 mm thick. The nominal design current is 21.5 kA at induction of 1.05 tesla in the gap. Thermal heating of this septum is rather low due to the short pulse width (1.5 ms). However, the mechanical stress due to magnetic pressure is rather severe. The septum is edge cooled by attaching two monel 400 rectangular tubes at the top and bottom of the septum. The resistance ratio of each tube to septun is only in the order of 0.27%; this results in nearly uniform current density in the septum. The septum is very carefully hand fitted into the magnet gap, so that the clearance between the septum and core can be kept at 0.025 mm. The laminations are made of intermediate silicone steel, 0.35 mm thick. The end plate is 31 mm thick, made of welded laminations. The laminations are held together by 4 ceramic insulated tie rods. The tightening torque is kept as low as possible (0.1 kG-m in our case). The stray field 6 mm from the middle of the septum was found to be 0.08% of the central internal field; 6 mm from the end of the septum the value was 1.4%.

III. External Optics

The design of the beam transport was dictated largely by the presence of two superconducting dipoles[5] at the 8° bend point located ~ 96 m from the ejector magnet and downstream of a 4½° bend with conventional magnets as shown in Fig. 2. The superconducting dipoles are 1.83 m long with a 7 cm ID vacuum pipe; the additional length of the dewar and vacuum chamber increased the length of the vacuum pipe to 2.62 m. Sagitta in the magnet accounted for 3.2 cm of the aperture. Calculations[6] indicate that as few as ~ 3 X 10^8 hadrons/cm^2/AGS cycle impinging on the Nb-Ti superconducting ribbon might cause the critical temperature to be exceeded and the magnet to revert to normal conductivity. It was therefore necessary to provide a beam of small horizontal size at this point with stability against momentum changes or variations in strength of the 4½° bend. We accomplished this by designing an achromatic system giving momentum recombination at the 8°; the five quadrupoles Q3 through Q7, between the 4½° and 8°, powered in series accomplish this objective. In addition, protective collimation upstream of the 8° bend was provided at a betatron phase shift of 180° at positions U5 and U12 in Fig. 2 to remove halo which might quench the superconductor. Antiscattering collimators were also provided at U170 and U259. The expected collimator images have been observed on scintillating screens upstream of the magnet, and the expected beam size there, 9 mm horizontal X 26 mm vertical, based on full extraction emittances of E_H= 2.42 π mm-mrad and E_V= 1.86 π mm-mrad, have been qualitatively confirmed.

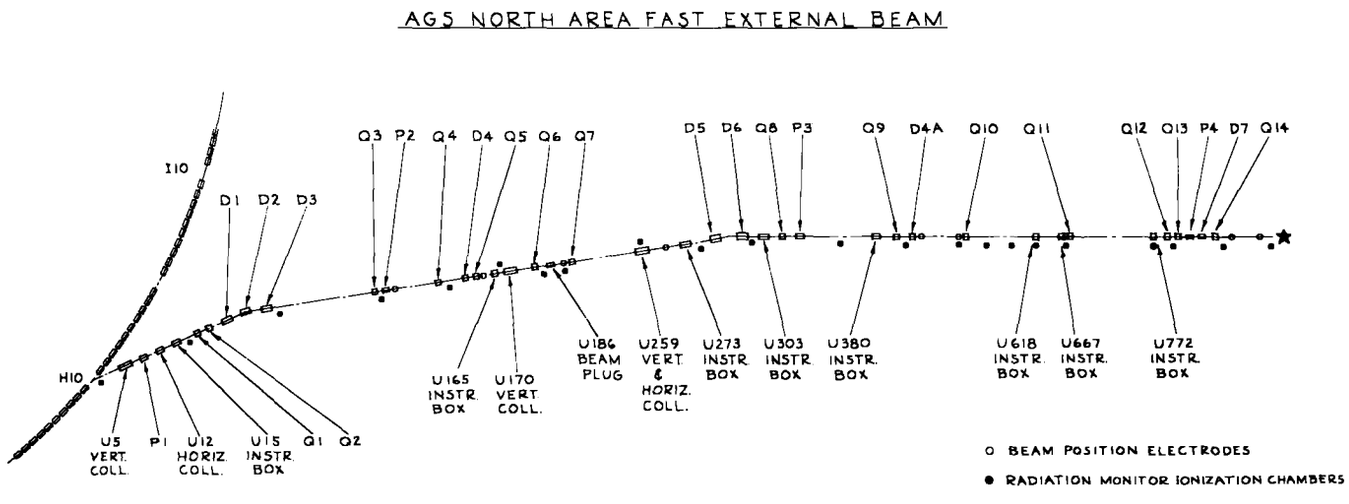

Fig. 2. Plan view of external beam line from ejector magnet to neutrino production target for 7-ft bubble chamber.

The transport downstream of the 8° is intended to provide a minimum spot size at the 5 mm dia. x 45.7 cm long sapphire production target. Qualitative observation on a BeO screen indicate that we have achieved the expected 1.7 mm horizontal x 1.2 mm vertical spot, which is minimum size for the given target length and emittances.

IV. Diagnostic Instrumentation

Instrumentation was designed to measure beam intensity, position and spatial distribution. All signals are presented as quasistatic analog levels at the computer interface. No electronic components are located within the primary radiation shield. Intensity is measured by current transformers at six locations. These consists of tape wound permalloy cores with n = 100 turn secondaries. The signal is fed via coaxial cable to an integrator/peak reader (Fig. 3). The integrators have an output calibration of

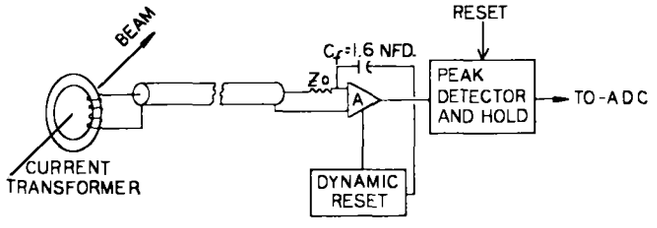

Fig. 3. Schematic diagram of beam current transformer and integrator.

$$Q/V = nC_f/1.6 \times 10^{-19} = 10^{12} \text{ protons/volt.} \quad (1)$$

The integrator incorporates a dynamic reset circuit which prevents runaway drift due to low source impedance but is slow enough (500 μs) to have a negligible effect over the 3 μs extraction interval. Bench calibration using a pulser or capacitor discharge source and a dielectric loaded coaxial fixture to minimize reflections showed less than 1% departure from the theoretical value in Eq. (1). Another calibration compared the integrator output with the beam charge determined from ^{11}C activation of polyethylene foils. This also agreed with the theoretical calibration to within the ± 4.6% uncertainty in the ^{11}C production cross section.[7] A current transformer with a 24 turn secondary has also been used to observe the temporal distribution of the beam (see Fig. 7 below).

Beam position is measured by insulated plates and split transverse ion chambers (STIC). Insulated plates in the AGS ring are situated in the shadows of the extraction magnet septa. The plates are charge sources by virtue of the knock-on electrons ejected by the proton beam. The efficiency is about 10%, i.e. one electron per 10 incident protons. The signal is transported via coaxial cable to integrators similar to those for current transformers; however, the peak detector and dynamic reset circuits are omitted because the source impedance is large. The plates are used to optimize extraction magnet position and skew-angle. Insulated plates are also located upstream of collimator jaws in the external transport, but suffer in this application due to ion collection in the rough vacuum (10^{-3} to 10^{-2} T). The residual gas ionization is exploited in the STIC (Fig. 4). The ions are propelled along field lines transverse to the beam axis to triangular collection electrodes. For uniform ionization density, the relative signal strength is proportional to beam position. The beam position is given by D·W/2, where W is the effective width of the electrodes and D is the normalized difference in integrated signals, (A-B)/(A+B).

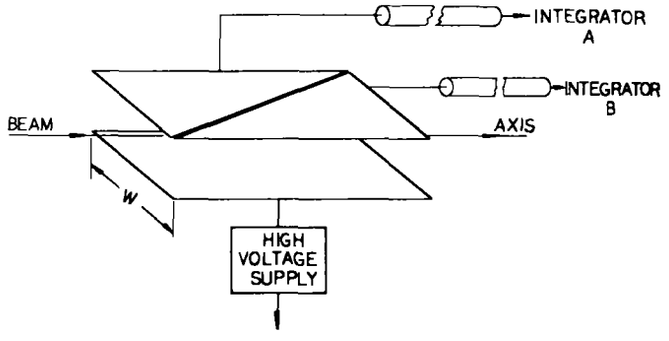

Fig. 4. Sketch of split transverse ion chamber (STIC).

Spatial distribution is provided by closed circuit TV viewing scintillating screens of "Radelin" (a fluoroscopy screen from U.S. Randium Corp.) or beryllium oxide, and by multiwire profile monitors. The usefulness of the screens is limited since they are easily damaged by the beam and optical and electronic components of the cameras suffer radiation damage. The profile monitors consist of 16 Al strips, 0.6 mm thick and 5 mm center-to-center spacing, attached to a rotatable frame. A 0.05 mm Al bias electrode is included upstream and downstream of the strips to comprise 16 parallel strip ionization chambers. Screens and profile monitors are mounted on remotely controlled actuators and are removed from the beam when not required. Future designs of the profile monitor will use thinner electrodes and bias foils. The charge from each electrode is stored on the coaxial signal cable which sees > 10^9 Ω impedance at the FET multiplex switch at the computer interface. In the "on" state, each switch FET has < 100 Ω resistance and the charge from each cable is sequentially transferred to an integrator and ADC. The read time per channel is 75 μs. The integrator gain is remotely varied over a 36:1 range by means of a switchable integrating capacitor. Typical beam profile displays are shown in Fig. 5.

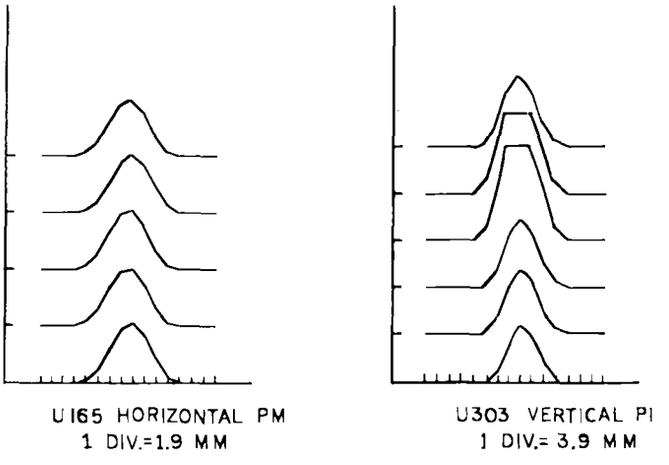

Fig. 5. Typical beam profile monitor displays for successive machine cycles. The profiles at right show saturation at low values for the remotely switched integrating capacitor.

We have also deployed 22 ionization chambers along the beam line to measure the longitudinal distribution of beam loss. The associated electronics include discriminators and alarm circuits which activate interlocks to turn the beam off should excessive losses occur. An illustration of the computer-generated loss pattern from these detectors is given in Fig. 6. The readout and display utilizes an amplifier and FET multiplex switch similar to the profile monitor circuit. The data readout and transfer is accomplished by a single-coax digital system, Datacon II, controlled by a PDP-8E computer interfaced to the AGS control room PDP-10 computer. The system is described elsewhere.[8]

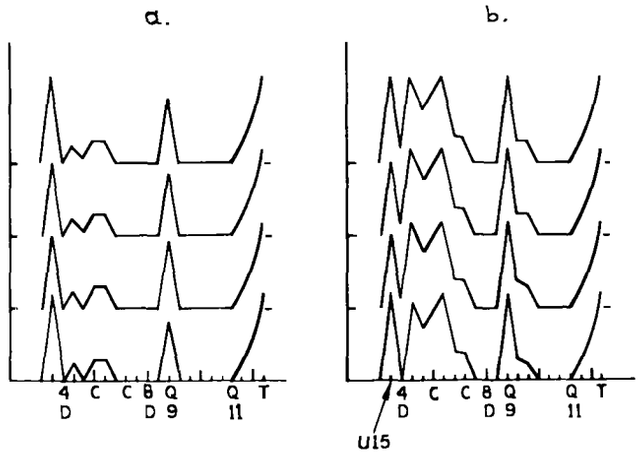

Fig. 6. Computer generated display of radiation monitor signals along the beam line. The ejector magnet is at the left, and the production target, T, at the right of each abscissa. a - Beam tuned for minimum loss. b - Scintillation screen (~ 72 mg/cm^2) inserted at U15.

V. Beam Performance

Extraction efficiency for the full extraction mode was measured by comparing the internal AGS "pick-up" electrode beam monitor to an external current transformer, and a monitor foil using carbon-eleven activation. During the calibration run, the measured efficiency was only 85%; however, ~ 90% is indicated by the current transformer at a circulating beam intensity of ~ 5 x 10^{12} when the beam is well tuned, and ~ 95% is observed at lower circulating beams of ~ 2 x 10^{12} p/p. Assuming that three AGS bunches are shaved by the E10 septum due to the finite rise time of the beam kicker pulse, the expected[9] theoretical efficiency is ~ 98%. Indirect evidence from bunch amplitudes from current transformer signals indicate an efficiency of 96%. Thus, the measurements are well within the ± 5% uncertainty in calibration of the internal beam monitor.[10]

Transport efficiency was measured by comparing current transformers and foil calibrations at the upstream and downstream end of the beam. The result under optimum conditions was 100 +0/-1%. Note that for this case, the coil activation results do not suffer from the ± 4% absolute uncertainty in the ^{11}C activation cross section.

The observed spill duration for total and fractional extraction in a bunched and unbunched mode were observed on an external current transformer and is shown in Fig. 7. For the full extraction case, it is seen that a fraction of the first bunch was shaved by the E10 septum; part of the remainder was extracted on the second turn. For the fractional extraction cases illustrated, the internal beam was only ~ 2 x 10^{12} p/p and we extracted about 25% of the beam. The spill duration for smaller fractions will be correspondingly less.

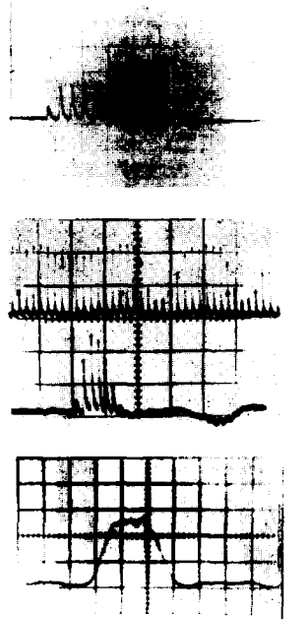

Fig. 7. Top photo - Oscillogram of external beam current transformer signal-full extraction mode, bunched beam (0.5 μsec/div). Middle photo - Fractional extraction mode, bunched beam. Upper trace shows AGS circulating beam intensity during extraction process. Lower trace shows external current transformer signal (1 μsec/div). Bottom photo - Current transformer oscillogram for fractional extraction mode, debunched beam (0.5 μsec/div).

The beam has been successfully utilized for both bubble chamber and spark chamber neutrino experiments. In these applications, position stability has been of importance for optimum neutrino production as well as to minimize neutron and muon background resulting from transport losses. We have noted that the position variation, ΔX, at an observation station ~ 14 m from the ejection magnet for a change, Δr, in the radial position of the internal beam is $\Delta X/\Delta r \approx 6.4$ mm/mm. The corresponding sensitivity at the production target is $(\Delta X)_{targ}/\Delta r = 2.2$ mm/mm. Thus, a radial shift Δr = 1 mm will move the spot at the production target by more than its diameter. We therefore had to optimize the gain of the AGS radial position servo, and have achieved long-term stability of $\Delta r \sim 0.1$ mm. Similarly, we have maintained the momentum drift at extraction time to 0.1% by careful adjustment of the motor-generator speed control. The extraction process is also sensitive to internal beam size. The beam size is in turn affected by longitudinal and transverse instabilities in the machine during acceleration. The instabilities are intensity and tune-dependent. We have observed both vertical and horizontal beam blow-up from coherent dipole oscillations and higher order resonances. To avert these difficulties, it is necessary to program the machine radius by a sequence of radius shifts during acceleration, as well as introduce a larger than optimal momentum spread by detuning the rf phase shift at transition energy. This procedure results in a beam loss at transition of ~ 15% from a circulating beam of ~ 6 x 10^{12} p/p. We also find that the available aperture at extraction time is only 3 mm. Typical machine tune at the extraction radius is $\nu_H = 8.74$, $\nu_V = 8.66$.

Spot size measurements in the external channel have been in qualitative agreement with calculations based on earlier emittance measurements.[11] However, we plan new measurements to define the emittance better under various extraction conditions. For the new measurements, we plan to measure the beam half widths, W_1, W_2 and W_3 at three different positions downstream of the 8° bend. It can be shown[12] the emittance area $\varepsilon = E/\pi$ and the ellipse parameter α_1 and β_1 at point one are given by

$$\varepsilon = \frac{\sqrt{(D_1 + D_2 + D_3)^2 - 2\,(D_1^2 + D_2^2 + D_3^2)}}{2|a_2b_3 - a_3b_2|b_2b_3} \qquad (2)$$

$$\alpha_1\varepsilon = \frac{\left[W_1^2\,(a_2^2b_3^2 - a_3^2b_2^2) - D_2 + D_3\right]}{2(a_2b_3 - a_3b_2)b_2b_3} \qquad (3)$$

$$\beta_1\varepsilon = W_1^2 \qquad (4)$$

where $D_1 = W_1^2\,(a_2b_3 - a_3b_2)^2$; $D_2 = W_2^2\,b_3^2$; $D_3 = W_3^2\,b_2^2$

and a_2, b_2 and a_3, b_3 are matrix elements of the transport matrix

$$M = \begin{pmatrix} a & b \\ c & d \end{pmatrix}$$

from point one to points two and three respectively.

Acknowledgements

We thank R. Adams and W. Gefers for the beam security system; R. Glasmann, J. Gabusi and E. Raka for valuable help in machine studies; D. Easler, W. Harrison and J. Schirmer for expert construction of external power supplies and computer interfaces; J. Balsamo, J. Guthy, E. Tombler and M. Zguris for invaluable contributions to the instrumentation; and A. Pendzick for excellent cooperation in facility installation. We are grateful for much support and consultations from J.G. Cottingham, B. Culwick, G. Danby, H. Foelsche, J. Grisoli, A. van Steenbergen and H. Williams.

References

1. L.N. Blumberg, J.G. Cottingham, J.W. Glenn, J.J. Grisoli, M. Month and A. van Steenbergen, Proc. U.S. Nat'l. Part. Accel. Conf., IEEE Trans. Nucl. Sci. NS-18, No. 3, 1009 (1971).
2. C. Bovet, D. Fiander, L. Henny, A. Krusche and G. Plass, Proc. U.S. Nat'l. Part. Accel. Conf., IEEE Trans. Nucl. Sci. NS-20, No. 3, 438 (1973).
3. J. Herrera, private communication, 1973.
4. E. Forsyth and C. Lasky, BNL Report BNL-910 (1965).
5. G. Danby et al., Proc. of this Conference.
6. Y.Y. Lee, BNL Accel. Dept. Int. Report EP&S 73-1 (1973).
7. J.B. Cumming et al., Phys. Rev. 125, 2078 (1962).
8. M.Q. Barton et al., Proc. of this Conference.
9. L. Blumberg and F. Krausz, BNL Accel. Dept. Int. Report, AGS DIV 71-1 (1971).
10. E.C. Raka, BNL Accel. Dept. Int. Report ECR-4 (1961); ECR-6 (1962).
11. L. Blumberg, M.Q. Barton, J.D. Fox, J.W. Glenn and L. Repeta, BNL Accel. Dept. Int. Report AGS DIV 69-12 (1969).
12. H. Ploss and L.N. Blumberg, BNL Accel. Dept. Int. Report AGS DIV 68-4 (1968).